ICAS 2021 SHANGHAI
International Council of the Aeronautical Sciences
32nd Congress of the International Council of the Aeronautical Sciences
September 6-10, 2021
Pudong Shangri-La, Shanghai, China

DESIGN OPTIMIZATION OF MULTIROTOR DRONES IN FORWARD FLIGHT

Félix Pollet[1], Scott Delbecq[1], Marc Budinger[2] & Jean-Marc Moschetta[1]

[1]ISAE-SUPAERO, Université de Toulouse, Toulouse, 31055, France
[2]ICA, Université de Toulouse, UPS, INSA, ISAE-SUPAERO, MINES-ALBI, CNRS, Toulouse, 31400, France

Abstract

The number of applications that use multirotor drones has significantly increased in the past year due to their high manoeuvrability and capability to perform hovering. The main limit of such configuration is its endurance especially when batteries are used as the energy source. This paper focuses on the evaluation of the endurance of multirotor drones in forward flight using a design optimization approach. Light-weight models to represent accuratly the physics of forward flight are proposed. One significant finding is that the design optimization code enables to rapidly obtain a design for a given set of requirements and has been validated on the Parrot ANAFI USA. The end of the article illustrates the sensitivity of maximum takeoff weight to the drag of aerodynamic frame.

Keywords: Multirotor Drone, UAV, Design optimization, Forward flight, MDO

1. Introduction

In recent years, multicopters have been increasingly used due of their ability to perform both hovering and complex maneuvers. These unique characteristics offer great potential for a wide range of applications such as delivery, inspection and emergency rescue missions. The missions thus performed by multirotor aerial vehicles (MRAVs) include forward flight phases, for which the operating conditions are different from other flight modes. According to [1, 2, 3], rotor performance changes significantly when the MRAV transitions from hover to forward flight. In addition, the airframe aerodynamics cannot be ignored as the speed increases [4, 5]. This poses new challenges for drone sizing, as it introduces new design drivers for the components [6, 7].

To date, most design and performance tools for multi-rotor UAVs do not consider forward flight, with hovering being the main sizing scenario for component selection. Among others, the online tools *ecalc* [8] and *flyeval* [9] allow to evaluate the performance of MRAVs but do not consider rotor aerodynamic changes in forward flight. Hwang et al. [10] proposed an endurance evaluation method to minimize the energy consumption of MRAVs in level flight, but the propeller efficiency is assumed to be constant with the flight speed. In [6], Ye et al. perform a propulsion optimization of a quadcopter in forward flight. However, the fuselage is of fixed size, so the design process is not applicable to drones of different scales. Oh et al. [11] developed a solution that enables the optimal design of multicopter drones including all flight modes. In this methodology, the propeller analysis is based on Blade Element Momentum Theory (BEMT), which requires the aerodynamic data and shape of the blades.

In this sense, this study proposes a model of an electric multicopter in the forward state and presents a sizing methodology that allows optimizing a configuration with flight distance and energy considerations. To this end, the paper is organized as follows. In section 2. the aerodynamic models of the MRAV are established and the component parameter models are recalled. In section 3. the optimization problem and the sizing procedure are presented. In section 4. the results of the design optimization are validated with an existing commercial quadcopter. Finally, a sensitivity study is performed in section 5. to investigate the effect of airframe drag on the components selection. Finally, section 6. offers concluding remarks.

Nomenclature

Latin Letters

C_d	Airframe Drag Coefficient	
C_l	Airframe Lift Coefficient	
C_P	Propeller Power Coefficient	
C_T	Propeller Thrust Coefficient	
D	Blade Diameter	m
D_f	Airframe Drag	N
J	Advance Ratio, $\frac{V_\infty}{nD}$	
J_{0T}, J_{0P}	Zero-Thrust and Zero-Power Advance Ratios	
J_{axial}	Axial Advance Ratio, $\frac{V_\infty}{nD} sin\alpha$	
L_f	Airframe Lift	N
N	Rotor Normal Force	N
N_{pro}	Number of propellers	
P	Rotor Power	N
S_{ref}	Reference surface of the UAV	m^2
S_{side}	Side surface of the UAV	m^2
S_{top}	Top surface of the UAV	m^2
T	Rotor Thrust	N
V_∞	Free-stream Velocity	m/s
V_c	Climb Velocity	m/s
W	Weight	N

Greek Letters

α	Rotor Disk Angle of Attack	rad
β	Blade Pitch Angle	rad
δ	Incidence Correction Factor	
η_T, η_P	Incidence Thrust and Power Ratios	
ρ_{air}	Density of Air	kg/m^3
θ_{FP}	Flight Path Angle	rad
n	Rotational Frequency	Hz

2. Multirotor modeling

2.1 Flight physics

Consider the equilibrium of forces on a multirotor drone in a climbing forward flight situation, as shown in Figure 1. In the figure V_∞ is the free stream velocity and V_c the climb velocity, so that θ_{FP} is the flight path angle of the drone [4]. The propellers angle of attack α is assumed to be same for each rotor k.

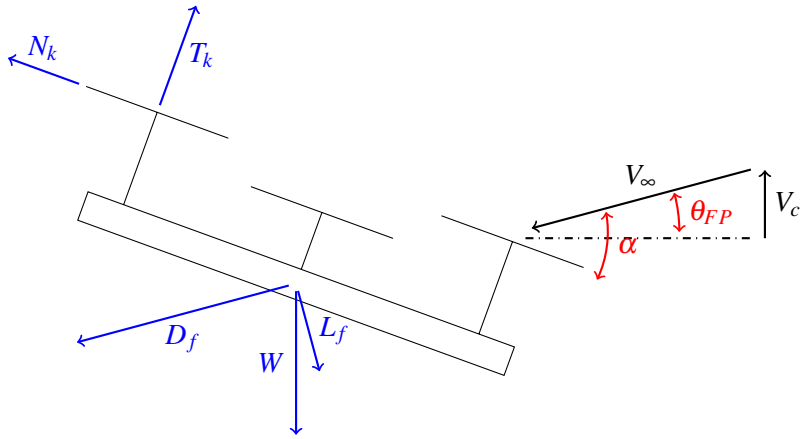

Figure 1 – Quadcopter in Climbing Forward Flight. Side view.

Satisfying the vertical equilibrium leads to

$$\sum_{k=1}^{N_{rotors}} T_k \cos(\alpha - \theta_{FP}) + N_k \sin(\alpha - \theta_{FP}) = W + D_f \sin\theta_{FP} + L_f \cos\theta_{FP} \tag{1}$$

where T_k, N_k are the thrust and normal force provided by the k^{th} rotor. The forces W, D_f and L_f represent the MRAV weight, parasitic drag and aerodynamic downwards force respectively.
Satisfying the horizontal equilibrium gives the equation

$$\sum_{k=1}^{N_{rotors}} T_k \sin(\alpha - \theta_{FP}) - N_k \cos(\alpha - \theta_{FP}) = D_f \cos\theta_{FP} - L_f \sin\theta_{FP} \tag{2}$$

Assuming all the rotors are identical and symmetrically positioned with respect to center of gravity of the drone, the tilt moment can be neglected and their operating regime considered as equal: $T_k = T$. In addition, the normal force N is neglected compared to the thrust T - as it is an order of magnitude lower [1].
The latter equations simplify to

$$N_{rotors} T \cos(\alpha - \theta_{FP}) = W + D_f \sin\theta_{FP} + L_f \cos\theta_{FP} \tag{3a}$$

$$N_{rotors} T \sin(\alpha - \theta_{FP}) = D_f \cos\theta_{FP} - L_f \sin\theta_{FP} \tag{3b}$$

Solving for the angle of attack α gives

$$\tan(\alpha - \theta_{FP}) = \frac{D\cos\theta_{FP} - L_f \sin\theta_{FP}}{W + D_f \sin\theta_{FP} + L_f \cos\theta_{FP}} \tag{4}$$

And, for the thrust

$$N_{rotors} T = \sqrt{(W + D_f \sin\theta_{FP} + L_f \cos\theta_{FP})^2 + (D\cos\theta_{FP} - L_f \sin\theta_{FP})^2} \tag{5}$$

The calculation of the parasitic drag D_f and lift L_f of the frame will be addressed further in this study. However, these quantities are functions of the angle of attack of the UAV, so that a numerical solver may be required to converge Equation 4.

2.2 Propellers with incidence angle

The rotor converts the energy output from the motor into aerodynamic forces that drive the MRAV. It is a key element to determine the efficiency of the propulsion chain. The performance of a propeller can be expressed as a function of its thrust and power coefficients — C_T and C_P respectively:

$$T = C_T \rho_{air} n^2 D^4 \tag{6a}$$

$$P = C_P \rho_{air} n^3 D^5 \tag{6b}$$

where ρ_{air} is the air density, n the rotational speed of the propeller and D its diameter.

The paper [12] has shown how surrogate modelling techniques can be used in order to obtain an analytic model of the propeller based on datasheets. Applying dimensional analysis and Buckingham theorem [13, 14], the authors proposed an expression of the thrust and power coefficients in axial flight conditions. It is a function of the axial advance ratio $J_{axial} = \frac{V_\infty \sin\alpha}{n.D}$ and the pitch-diameter ratio β of the propeller:

$$C_{T,P}^{axial} = f(\beta, J_{axial}) \tag{7}$$

An approximation of the function f was then achieved by performing data regressions on filtered APC propellers datasheets [15]. A 3^{rd} order polynomial model was retained for both thrust and power coefficients:

$$\begin{aligned} C_T^{axial} =& 0.02791 - 0.06543 J_{axial} + 0.11867\beta + 0.27334\beta^2 - 0.28852\beta^3 \\ &+ 0.02104 J_{axial}^3 - 0.23504 J_{axial}^2 + 0.18677\beta J_{axial}^2 \end{aligned} \tag{8a}$$

$$\begin{aligned} C_P^{axial} =& 0.01813 - 0.06218\beta + 0.00343 J_{axial} + 0.35712\beta^2 - 0.23774\beta^3 \\ &+ 0.07549\beta J_{axial} - 0.1235 J_{axial}^2 \end{aligned} \tag{8b}$$

However, this model is valid in axial conditions only. For a multicopter in forward flight, the propeller incidence angle could range between 0 and 90 degrees. The aerodynamic coefficients thus need to be modified accordingly. In [1], Leng et al. proposed an analytical model to express thrust and power coefficients at non-zero incidence angle as ratios to their respective values in axisymmetric conditions. For a given blade geometry the authors suggested the following expressions:

$$C_{T,P}(\alpha, J) = \eta_{T,P}(\alpha) C_{T,P}(0, J_{axial}) \tag{9a}$$

$$\eta_{T,P}(\alpha) = 1 + \frac{(J\cos\alpha/\pi\bar{r}')^2}{2(1 - J\sin\alpha/J_{0T,P}^{axial})}\delta(\alpha) \tag{9b}$$

Where

- α is the angle of attack as defined in Figure 1
- $J = \frac{V_\infty}{n.D}$ is the advance ratio
- $J_{0T,P}^{axial}$ are the axial advance ratios where the thrust and power coefficients reach zero respectively. These ratios can be obtained from Equation 8.
- $\bar{r}'$ is the position of representative section of the blade, in percentage radius (taken as 75%)
- $\delta(\alpha)$ is a solidity term correction

For further details, interested readers are kindly referred to the publication from Leng et al. [1].
The estimated C_T and C_P for a fixed pitch $\beta = 0.3$ APC propeller are depicted in Figure 2.

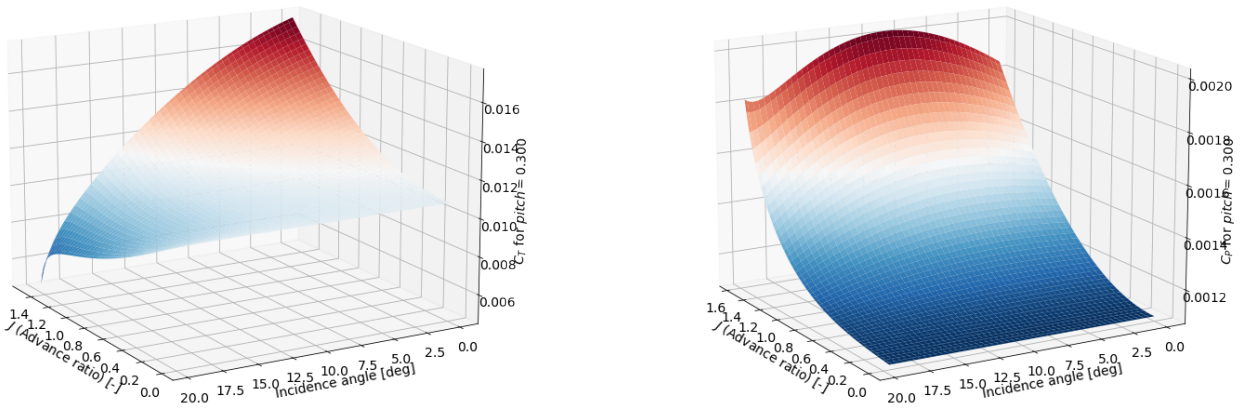

(a) 3D plot of C_T

(b) 3D plot of C_P

Figure 2 – 3D models of estimated performance coefficients for a propeller derived from APC data - $\beta = 0.3$

2.3 Body frame aerodynamics

The drag D_f and lift L_f of the frame when the MRAV is in forward flight can be written as:

$$D_f = \frac{1}{2} C_d \rho_{air} V_\infty^2 S_{ref} \tag{10a}$$

$$L_f = \frac{1}{2} C_l \rho_{air} V_\infty^2 S_{ref} \tag{10b}$$

As depicted in Figure 1, L_f acts as a downward force when the drone moves forward — the aerodynamic surfaces on a multicopter are mostly disadvantageous.
The effective drag area S_{ref} varies with the angle of attack and the surfaces facing the relative wind.

$$S_{ref} = S_{top} \sin\alpha + S_{front} \cos\alpha \tag{11}$$

The evaluation of the planar areas of the airframe are derived from scaling laws based on dimensional analysis. Under the assumption of geometrical similarity, i.e. the frame length ratios from one airframe to another are constant, and considering that the drone mass is the main driver of these dimensions then:

$$\frac{S_{top}}{S_{top,ref}} = \left(\frac{M}{M_{ref}}\right)^{2/3} \tag{12a}$$

$$\frac{S_{front}}{S_{front,ref}} = \left(\frac{M}{M_{ref}}\right)^{2/3} \tag{12b}$$

where $S_{top,ref}$, $S_{top,ref}$ and M_{ref} are the properties of a reference MRAV. In the following Figure 3, surfaces data from several multicopters [16] are compared with their corresponding scaling laws. The reference MRAVs are represented in red.
The deviations can be explained by the diversity of airframe shapes that can be found on the market and by the different missions for which the multicopters are designed. However, it remains acceptable for a preliminary model.

The drag coefficient C_d and lift coefficient C_l depend highly on the body shape. Other parameters such as the flow direction and the Reynold's number impact their value. In this research, these coefficients are considered constant. In addition, the interferences between the rotor and the fuselage are neglected, as indicated by Luo [17].

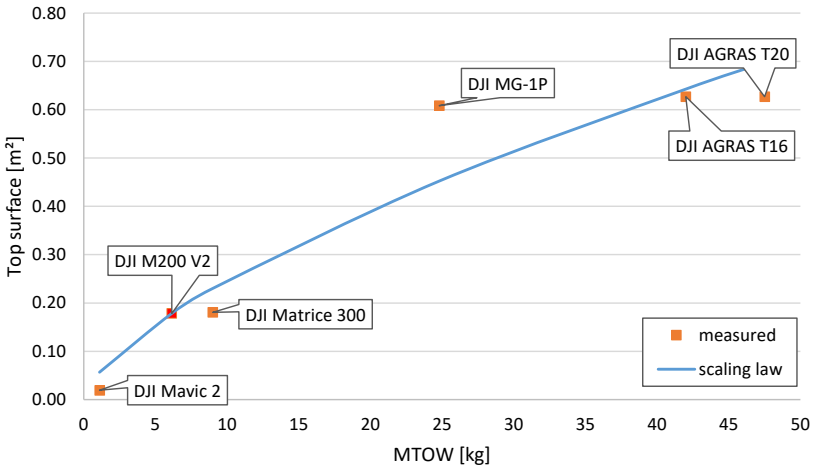

(a) Top surface variation with Maximum Take-Off Weight

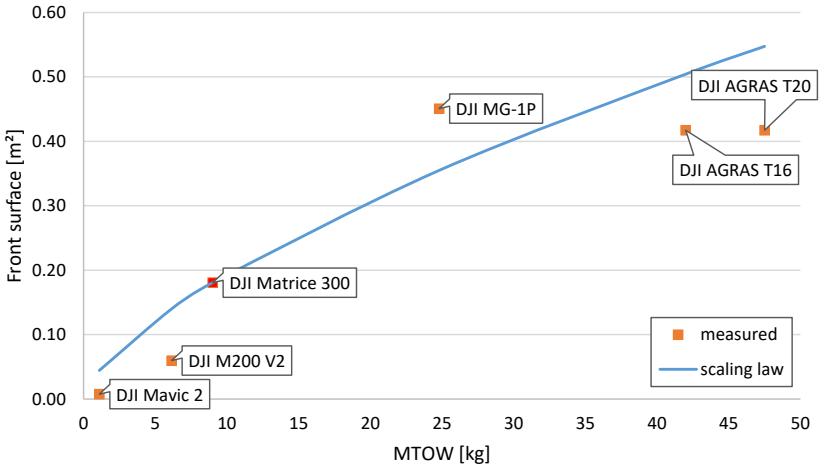

(b) Front surface variation with Maximum Take-Off Weight

Figure 3 – Frame surfaces vs Maximum Take-Off Weight for several DJI multicopters [16].

As shown in the examples of Baker et al. [18], the value of C_d is 0.47 for a sphere, 1.05 for a cube, and 2.05 for a long rectangular body with Reynolds number approximately 10^4. In [6], Ye et al. proposed an aerodynamic model for a hollow fuselage of a quadcopter in forward state. However, it is constructed using CFD methods applied to a self-designed drone, and is thus not applicable for preliminary design of a generic system. In [19], the authors use high-fidelity CFD methods to analyze a quadcopter specialized for forward flight, the SUI Endurance [20]. The results show that for the entire structure (including the fuselage, landing gear, canards and arms) a drag coefficient of $C_d = 0.425$ and a beneficial lift with $C_l = 0.193$ are obtained. It is worth mentioning that the SUI Endurance fairing has been optimized to minimize drag and provide lift in forward flight mode, which is not the case for most multicopter designs.
The uncertainties on drag coefficient on the final design of the UAV is evaluated in section 5.

2.4 Electrical components

A set a continuous models for the key electrical components is presented in paper [12]. The main scaling laws for the battery, Electronic Speed Controller (ESC) and motors are presented in the following Table 2. Interested readers are kindly reffered to Budinger et al. paper for further details [12]. The use of such models is intented to facilitate the selection procedure of the components in

the overall drone sizing process, as presented in [21].

Table 2 – Scaling laws for electrical components [12].

Parameters	Equation
Motor mass	$M_{mot} = M_{mot,ref} \left(\frac{T_{mot}}{T_{mot,ref}} \right)^{3/3.5}$
Motor maximum torque	$T_{max,mot} = T_{max,mot,ref} \frac{T_{mot}}{T_{mot,ref}}$
Motor friction torque	$T_{mot,fr} = T_{mot,fr,ref} \left(\frac{T_{mot}}{T_{mot,ref}} \right)^{3/3.5}$
Motor resistance	$R_{mot} = R_{mot,ref} \left(\frac{K_{T,mot}}{K_{T,mot,ref}} \right)^{2} \left(\frac{T_{mot}}{T_{mot,ref}} \right)^{-5/3.5}$
Motor inertia	$J_{mot} = J_{mot,ref} \left(\frac{T_{mot}}{T_{mot,ref}} \right)^{5/3.5}$
ESC voltage	$V_{esc} = V_{esc,ref} \left(\frac{P_{esc}}{P_{esc,ref}} \right)^{1/3}$
ESC mass	$M_{esc} = M_{esc,ref} \frac{P_{esc}}{P_{esc,ref}}$
Battery max. current	$I_{max,bat} = I_{max,bat,ref} \frac{C_{bat}}{C_{bat,ref}}$
Battery mass	$M_{bat} = M_{bat,ref} \frac{C_{bat}}{C_{bat,ref}} \frac{U_{bat}}{U_{bat,ref}}$
Battery energy	$E_{bat} = E_{bat,ref} \frac{M_{bat}}{M_{bat,ref}}$

3. Optimization problem

3.1 Problem definition

The analytical models of the components presented in this article allow performing a preliminary design of electric multicopters. In [21], Delbecq et al. propose an efficient sizing methodology which allows to optimize a configuration for potentially very different missions and requirements. However, no consideration is given to the forward flight scenario, so that the design drivers to select the system components are associated with the three following scenarios: take-off, hovering flight, maximum climb rate. In this research, additional focus is set on the forward flight.

When it comes to optimization, the objective is to find the best system design satisfying a set of requirements by manipulating the values of design parameters. It is an iterative process that requires the definition of design variables, consistency constraints and an objective function. The optimization problem for multirotor drones with forward flight considerations can be expressed as follows:

$$\begin{array}{ll} \text{minimize} & E_{tot}(x) \\ \text{with respect to} & x = J, V_\infty, k_i \; i = 1, \ldots, m. \\ \text{subject to} & R(x) \geq R_{spec} \\ & f_j(x) \leq c_j \; j = 1, \ldots, n. \end{array} \tag{13}$$

Here, the objective is to minimize the total energy E_{tot} of the mission with a minimum range R_{spec} requirement. The design variables k_i are defined in [21] and represent component-specific sizing coefficients. Additionally, the advance ratio $J = \frac{V_\infty}{nD}$ is introduced in this research to take account for the rotor operating condition in forward flight. The freestream velocity V_∞ can be set either as a specification or a design variable. In the latter case, the speed of the drone will be optimized together with its design. Finally, the constraints $f_j(x) \leq c_j$ ensure the consistency of the system to satisfy the lift and power requirements for the different flight scenarios. A detailed description of the initial optimization problem can be found in [21] which is implemented and solved in FAST-OAD [22], an OpenMDAO based framework [23].

Another possible objective is to maximize the range R that can be reached by the multicopter. In that

case, an upper value for the Maximum Take-Off Weight, $M_{tot,spec}$, can be specified by the user.

$$\begin{aligned} &\text{maximize} && R(x) \\ &\text{with respect to} && x = J, V_\infty, k_i \; i = 1, \ldots, m. \\ &\text{subject to} && M_{tot}(x) \leq M_{tot,spec} \\ & && f_j(x) \leq c_j \; j = 1, \ldots, n. \end{aligned} \tag{14}$$

3.2 Sizing procedure

The selection of the components relies on the definition of sizing scenarios which are part of the specification process. Once the required thrust for the missions is estimated, propeller torque and speed are calculated. These values are used to evaluate the motor parameters and so on for the ESC, battery and frame parameters. Finally, the objective function is evaluated and an optimization algorithm is responsible for iterating the process until the best design is reached.
Delbecq et al. [21] proposed an efficient implementation of the sizing procedure to reduce the problem complexity and the resolution time. It makes use of the monotonicity analysis [24] and the Normalized Variable Hybrid (NVH) formulation. The sizing procedure is illustrated in Figure 4, where k_i are the design variables, C_j are the inequality constraints, and f is the objective function. This flowchart follows the eXtended Design Structure Matrix (XDSM) notation [25] to visualize the models involved and the shared variables. Green boxes represent generic processes, while parallelograms are used for data inputs and outputs. The blue rounded rectangle refers to the main optimization driver, responsible for the iteration loop by evaluating the cost function and changing the design parameters.

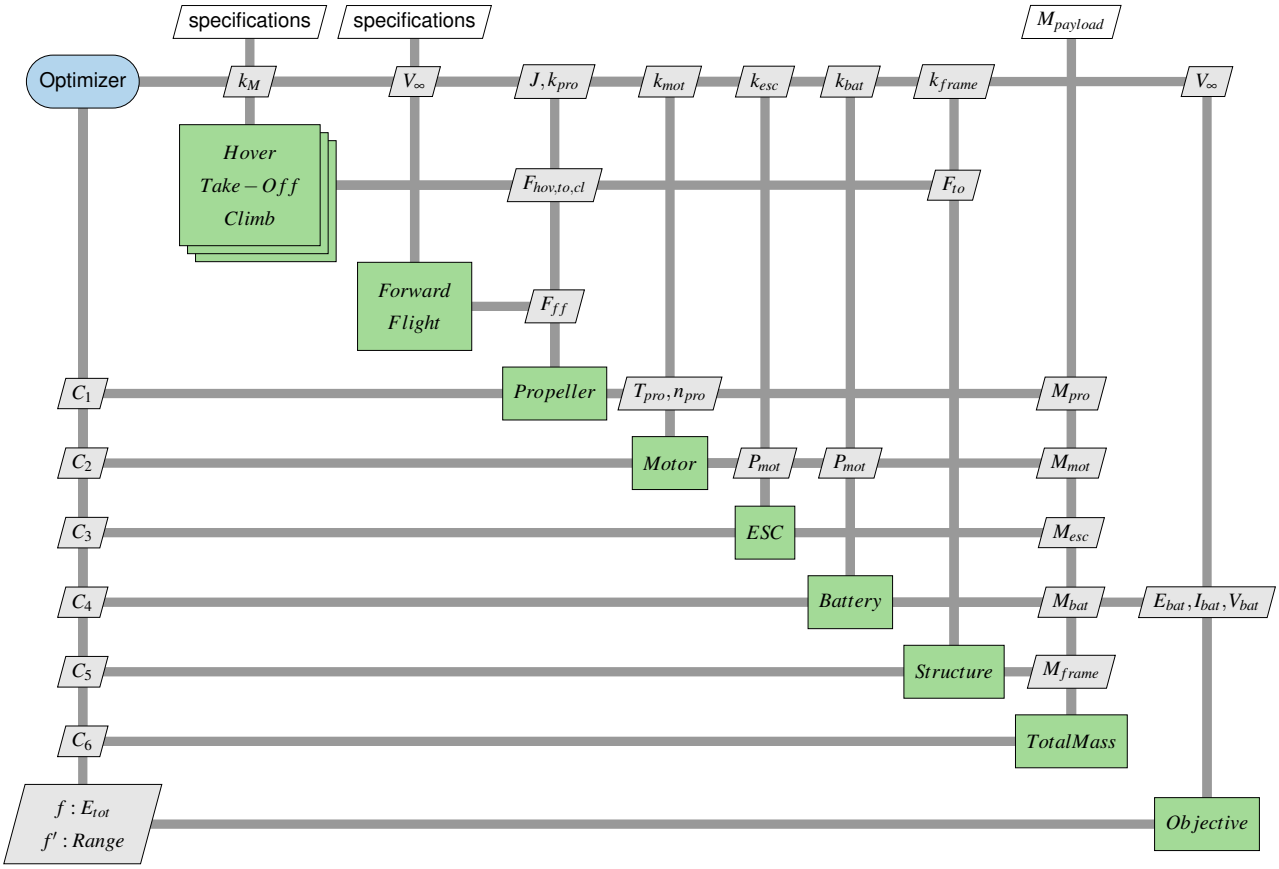

Figure 4 – XDSM diagram for multirotor drone optimization.

4. Validation

To validate the results obtained with the overall sizing optimization, a quadrotor drone from Parrot is used: the *Parrot ANAFI USA* [26]. It offers a theoretical range of 17.4 km for a Maximum Take-Off

Weight (MTOW) of 500 grams, and features a triple camera module.
The optimization process is configured to maximize the flight distance in straight and level flight with a maximum mass constraint, as defined in Equation 14. The lift generated by the fuselage is not taken into account here due to the lack of data.
Table 4 shows the results for different components and flight parameters. The calculated characteristics are close to the manufacturer's data, with small deviations for the outreach and the associated flight speed: -1.1% and +6.2% respectively. The discreprancies observed for the surfaces are probably due to the architectural choices for the layout of the components in the bodyframe.
The optimization was successfully completed in 3.06 seconds and 18 iterations on a Intel Core i7-10610U CPU.

Parrot ANAFI USA

Figure 5 – Parrot ANAFI USA. Source: [26].

Table 3 – Specifications for design optimization.

MTOW:	500 grams
Payload mass:	250 grams
Payload consumption:	15 W
Max. vertical acceleration:	2.5 g
Airframe C_d:	1.0

Table 4 – Comparison of results for the Parrot ANAFI USA.

	Reference	Sizing	Rel. Error [%]
Range [km]	17.4	17.2	-1.1
Optimal Velocity [m/s]	11.3	12.0	+6.2
Battery energy [Wh]	40.0	42.2	+5.5
Battery mass [g]	195	183	-6.2
Top surface [m^2]	0.026	0.023	-11.5
Front surface [m^2]	0.009	0.010	+11.1

5. Sensitivity study: effect of the airframe aerodynamics

The airframe aerodynamics of the MRAV is an important aspect of forward flight performance, as explained in Section 2. Although the drag and lift forces on the fuselage can be ignored in hovering flight, it increases greatly with forward speed. As a consequence, uncertainties on these parameters result in approximation errors in the performance evaluation.
To investigate this effect, we focus on varying the aerodynamic coefficient C_d to satisfy the energy minimization objective with a flight distance requirement (Equation 13). The main specifications for this study are shown in Table 5. In this part, we focus on an octocopter configuration designed for a

5 kg payload and a range of 20 km.
The mass breakdown Figure 6 shows how a higher drag coefficient implies an increase in the mass of the configuration. This is mainly due to the battery, as the other components remain quite unchanged. This is because the forward speed of the multicopter is optimized to reach the flight distance, such that almost no power increase in the propulsion chain is required to maintain the straight and level flight. Figure 7 shows the evolution of optimal flight speed with C_d. As the drag coefficient increases, the optimum speed is reduced.

Table 5 – Specifications for design optimization.

Number of arms:	8
Number of propeller per arm:	1
Payload mass:	5 kg
Max. vertical acceleration:	2 g
Design range:	20 km

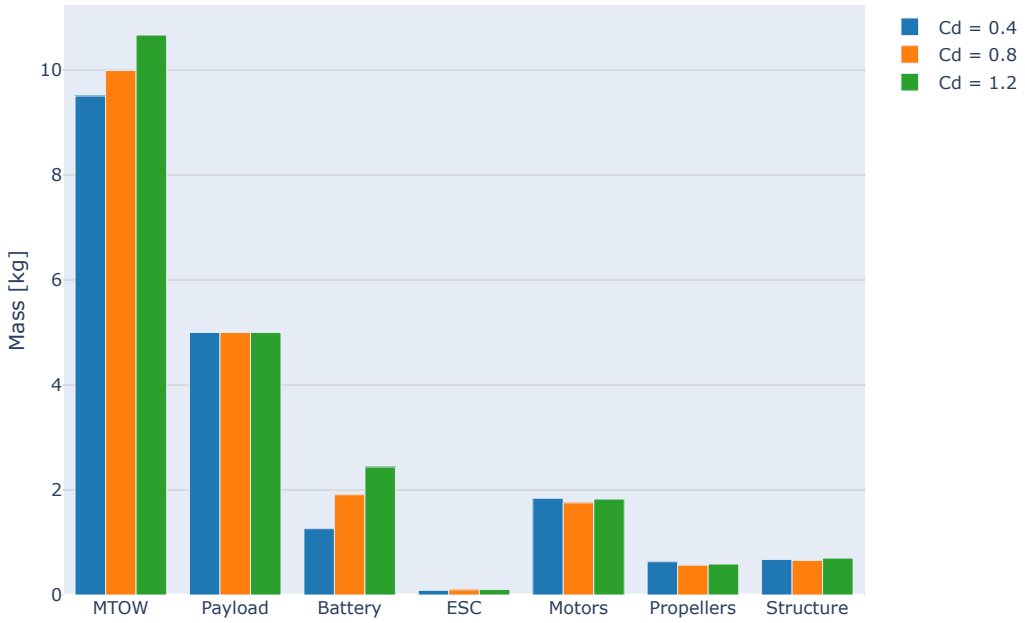

Figure 6 – Evolution of the component's masses with respect to the airframe drag coefficient.

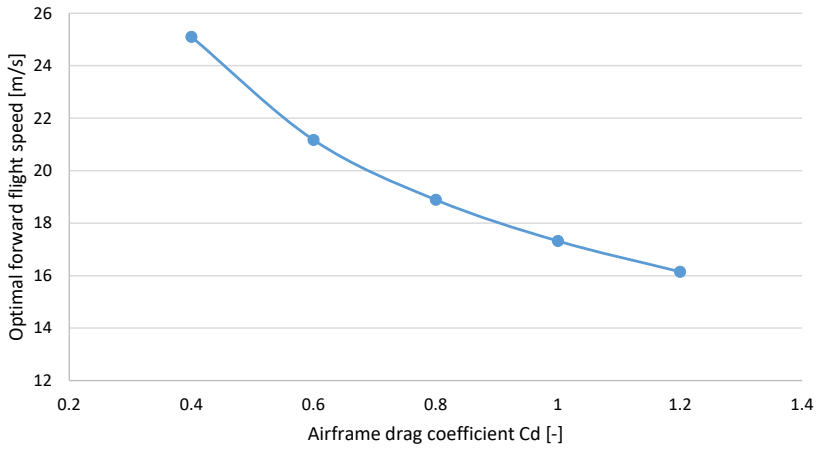

Figure 7 – Evolution of the optimal flight speed with respect to the airframe drag coefficient.

6. Conclusions

In this study, a design optimization of multicopter drones is carried out on the basis of forward flight considerations. The aerodynamic models specific to this flight mode were presented and applied in a design optimization approach. In particular, the variation of propeller performance in off-axis conditions is performed. The results obtained with the sizing procedure were then validated on a quadcopter from the consumer market. Finally, a sensitivity study has shown to what extent a more aerodynamic airframe reduces the total mass of a drone designed for a specific mission. The accuracy of the design could be improved by linking the sizing tool to CFD methods or low-fidelity models of the fuselage aerodynamics.

7. Copyright Statement

References

[1] Y. Leng, J.-M. Moschetta, T. Jardin, and M. Bronz, "An analytical model for propeller aerodynamic efforts at high incidence," Mar. 2019.

[2] R. Gill and R. D'Andrea, "Propeller thrust and drag in forward flight," in *2017 IEEE Conference on Control Technology and Applications (CCTA)*, (Mauna Lani Resort, HI, USA), pp. 73–79, IEEE, Aug. 2017.

[3] Y. Yang, Y. Liu, Y. Li, E. Arcondoulis, and Y. Wang, "Aerodynamic and Aeroacoustic Performance of an Isolated Multicopter Rotor During Forward Flight," *AIAA Journal*, vol. 58, pp. 1171–1181, Mar. 2020.

[4] J. G. Leishman, *Principles of Helicopter Aerodynamics*. Cambridge University Press, Dec. 2002.

[5] M. Schulz, F. Augugliaro, R. Ritz, and R. D'Andrea, "High-speed, steady flight with a quadrocopter in a confined environment using a tether," in *2015 IEEE/RSJ International Conference on Intelligent Robots and Systems (IROS)*, (Hamburg, Germany), pp. 1279–1284, IEEE, Sept. 2015.

[6] J. Ye, J. Wang, T. Song, Y. Zhu, Z. Wu, and P. Tang, "Propulsion optimization of a quadcopter in forward state," *Aerospace Science and Technology*, vol. 113, p. 106703, June 2021.

[7] D. Shi, X. Dai, X. Zhang, and Q. Quan, "A Practical Performance Evaluation Method for Electric Multicopters," *IEEE/ASME Transactions on Mechatronics*, vol. 22, pp. 1337–1348, June 2017.

[8] eCalc. `https://www.ecalc.ch`. (Accessed 2021-05-28).

[9] flyeval, "Flight Evaluation." `https://www.flyeval.com`. (Accessed 2021-05-28).

[10] M.-h. Hwang, H.-R. Cha, and S. Y. Jung, "Practical Endurance Estimation for Minimizing Energy Consumption of Multirotor Unmanned Aerial Vehicles," *Energies*, vol. 11, p. 2221, Aug. 2018.

[11] S. Oh, M. Kim, H. Kim, D. Lim, K. Yee, and D. Kim, "The Solution Development for Performance Analysis and Optimal Design of Multicopter-type Small Drones," in *2020 International Conference on Unmanned Aircraft Systems (ICUAS)*, pp. 975–982, Sept. 2020. ISSN: 2575-7296.

[12] M. Budinger, A. Reysset, A. Ochotorena, and S. Delbecq, "Scaling laws and similarity models for the preliminary design of multirotor drones," *Aerospace Science and Technology*, vol. 98, p. 105658, Mar. 2020.

[13] M. H. Holmes, "Dimensional Analysis," in *Introduction to the Foundations of Applied Mathematics* (M. H. Holmes, ed.), Texts in Applied Mathematics, pp. 1–42, New York, NY: Springer, 2009.

[14] E. van Groesen and J. Molenaar, *Continuum Modeling in the Physical Sciences*. Philadelphia, PA: Society for Industrial and Applied Mathematics, Jan. 2007.

[15] A. propellers, "Performance data." `https://www.apcprop.com/technical-information/performance-data/`. (Accessed 2021-05-28).

[16] DJI. `https://www.dji.com`. (Accessed 2021-05-28).

[17] J. Luo, L. Zhu, and G. Yan, "Novel Quadrotor Forward-Flight Model Based on Wake Interference," *AIAA Journal*, vol. 53, pp. 1–12, Oct. 2015.

[18] W. Baker, P. Cox, J. Kulesz, R. Strehlow, and P. Westine, "Loading from Blast Waves," in *Fundamental Studies in Engineering*, vol. 5, pp. 222–272, Elsevier, 1983.

[19] P. Ventura Diaz and S. Yoon, "High-Fidelity Computational Aerodynamics of Multi-Rotor Unmanned Aerial

Vehicles," in *2018 AIAA Aerospace Sciences Meeting*, (Kissimmee, Florida), American Institute of Aeronautics and Astronautics, Jan. 2018.

[20] H. C. Solutions, "SUI Endurance." https://hitecnology.com/drones/sui-endurance-multipurpose-professional-multirotor. (Accessed 2021-05-28).

[21] S. Delbecq, M. Budinger, A. Ochotorena, A. Reysset, and F. Defay, "Efficient sizing and optimization of multirotor drones based on scaling laws and similarity models," *Aerospace Science and Technology*, vol. 102, p. 105873, July 2020.

[22] C. David, S. Delbecq, S. Defoort, P. Schmollgruber, E. Benard, and V. Pommier-Budinger, "From fast to fast-oad: An open source framework for rapid overall aircraft design," in *IOP Conference Series: Materials Science and Engineering*, vol. 1024, p. 012062, IOP Publishing, 2021.

[23] J. S. Gray, J. T. Hwang, J. R. R. A. Martins, K. T. Moore, and B. A. Naylor, "OpenMDAO: an open-source framework for multidisciplinary design, analysis, and optimization," *Structural and Multidisciplinary Optimization*, vol. 59, pp. 1075–1104, Apr. 2019.

[24] P. Y. Papalambros and D. J. Wilde, *Principles of Optimal Design: Modeling and Computation*. Cambridge University Press, July 2000.

[25] A. B. Lambe and J. R. R. A. Martins, "Extensions to the design structure matrix for the description of multidisciplinary design, analysis, and optimization processes," *Structural and Multidisciplinary Optimization*, vol. 46, pp. 273–284, Aug. 2012.

[26] Parrot, "ANAFI USA." https://www.parrot.com/us/drones/anafi-usa. (Accessed 2021-05-28).